A storyline approach to select the CMIP6 model ensemble to be downscaled for the South America domain

Climate Dynamics (2026) 64:82
https://doi.org/10.1007/s00382-025-08017-8

ORIGINAL ARTICLE

A storyline approach to select the CMIP6 model ensemble to be downscaled for the South America domain

Andressa A. Cardoso[1,2,3] · **Julia Mindlin**[4,5,6,7] · **Erika Coppola**[2] · **Theodore G. Shepherd**[3,8]

Received: 15 May 2025 / Accepted: 7 December 2025

Abstract
Selecting the most appropriate Global Climate Models (GCMs) is necessary for Regional Climate Models (RCMs) downscaling. We propose a methodology to select CMIP6 GCMs based on the representation of the multiple physical processes which control regional circulation in a specific domain and the uncertainty in the precipitation projections. To develop the methodology, we identified relevant climate features for the South American (SA) region, focusing on the two most important climatological features: the South American Monsoon System (SAMS) and extratropical cyclones. A set of indicators was defined based on the precipitation in three specific regions (the La Plata and Amazon basins, and Southeastern Brazil) and circulation patterns that are part of the SAMS and control the tracking of extratropical cyclones (South American Low-Level jets, South Atlantic and South Pacific Subtropical Highs, trade winds, Bolivian High, cyclonic vortices, and upper-level jet stream). The selection of the CMIP6 GCM ensemble is based on historical validation of the circulation patterns and the spread in possible future circulation changes that can lead to different precipitation responses. We used a storyline approach to assess the spread in the precipitation response controlled by regional circulation uncertainty and to identify the wettest and driest possible futures. To assess both SAMS (in summer) and extratropical cyclone patterns (in summer and winter), three storylines were used. The final proposed minimal ensemble comprises four CMIP6 GCMs that correctly represent the main climatological features in SA and are able to cover the uncertainty in the future precipitation response in the three examined regions.

Keywords CMIP6 GCMs selection · Downscaling · South America · Circulation uncertainty · Future outcomes

1 Introduction

Given the great demand for actionable climate information, research on climate change impacts at a regional scale has progressed in the last decade. The signature of global warming at the regional scale has been one of the focuses of the latest Intergovernmental Panel on Climate Change (IPCC) Sixth Assessment Report (AR6), and one of the main outcomes was that regional climate changes can affect multiple climatic impact drivers (WGI IPCC AR6 2023). The

✉ Andressa A. Cardoso
cardoso.andressa.andrade@gmail.com

1 Instituto de Astronomia, Departamento de Meteorologia, Geofísica e Ciências Atmosféricas - IAG, Universidade de São Paulo, São Paulo, Brazil

2 The Abdus Salam International Centre for Theoretical Physics – ICTP, Earth System Physics Department, Trieste, Italy

3 Department of Meteorology, University of Reading, Reading, UK

4 Departamento de Ciencias de la Atmósfera y los Océanos, Universidad de Buenos Aires, Buenos Aires, Argentina

5 Centro de Investigaciones del Mar y la Atmósfera, Consejo Nacional de Investigaciones Científicas y Técnicas, Universidad Nacional de Buenos Aires, Buenos Aires, Argentina

6 Instituto Franco Argentino sobre estudios de Clima y sus impactos (IFAECI-UMI3351), Centre National de la Recherche Scientifique, Buenos Aires, Argentina

7 Leipzig Institute for Meteorology, Leipzig University, Leipzig, Germany

8 Jülich Supercomputing Centre, Forschungszentrum Jülich, Jülich, Germany

Published online: 05 February 2026

analysis in the reports of the IPCC relies on data and projections from Global Climate Models (GCMs) developed under the Coupled Model Intercomparison Project (CMIP) and regional climate projections. The CMIP is a coordinated project to improve the knowledge of past and future climates by means of coupled model projections completed by different modelling groups worldwide. In recent years, the CMIP has increased the number of models, as well as the kind of experiments and number of future scenarios and has improved the models in each of the cycles (Eyring et al. 2016).

Nevertheless, GCMs simulate climate projections at the global scale with a resolution that is not suitable for studying processes at the regional scale. To address this, Regional Climate Models (RCMs) can be used instead to provide higher resolution information more suitable for the application to impacts and adaptation studies at regional scales (Giorgi 2019).

Lateral boundary conditions needed to run RCMs are derived from the available GCM simulations. Running RCMs is computationally expensive and not all the GCMs show reasonable performance in representing large-scale circulations in all regions of the world (McSweeney et al. 2015). This makes the informed selection of available GCMs for downscaling purposes a fundamental step in the process. Therefore, a justified selection criteria must be based on the performance of CMIP6 GCMs in representing the relevant physical processes of the regional circulation for the specific domain of interest. Moreover, uncertainty in the CMIP ensemble projections at the regional scale is controlled by model uncertainty, especially regional precipitation uncertainty which is controlled by the uncertainty in the forced circulation response (Shepherd 2014). In order to represent this source of uncertainty with a small RCM ensemble, the selection criteria must also consider models with different yet plausible regional circulation changes.

Selecting a subset of models by evaluating the ability of GCMs in a historical period and the spread of uncertainty for temperature and precipitation projections could be a good approach, and has already been used in several studies to select CMIP5 GCMs in specific regions (McSweeney et al. 2015; da Silva et al. 2022) as well as for CMIP6 (Olmo et al. 2022; Di Virgilio et al. 2022; Palmer et al. 2023; Zhang et al. 2024; Arias et al. 2025). For this purpose, a storyline approach can be used to evaluate the regional responses that are associated with multiple plausible future climates (Shepherd et al. 2018). One approach to addressing this issue involves representing the uncertainty in the atmospheric circulation response based on a selection of remote drivers that capture the most relevant and uncertain features (Zappa and Shepherd 2017). With this approach, different plausible futures are identified and articulated in terms of the response to forcing of regional circulation drivers and the sensitivity to this uncertainty in a variable of interest like precipitation, as used in this work.

Several large-scale circulation features on the South American (SA) continent are relevant for the evolution of many meteorological variables in the region, together with several geographical features that shape the climate of this region (Silva and Kousky 2012). For instance, the continent is surrounded by ocean (Atlantic and Pacific subtropical oceans) that contributes to the moisture transport into the continent; the Andes mountain contributes to deflecting the low-level easterly winds (Vera et al. 2006b); the Amazon Basin contains the largest rainforest of the world; and the north of Chile holds the Atacama desert (Silva and Kousky 2012). The two most important atmospheric systems that impact the precipitation variability over SA are the South American Monsoon System (SAMS, da Silva and de Carvalho 2007; Marengo et al. 2010; Silva and Kousky 2012; Llopart et al. 2014), and extratropical cyclones (Hoskins and Hodges 2005; Reboita et al. 2010a; Gramcianinov et al. 2019; Crespo et al. 2020).

The main aim of the paper is to select which CMIP6 GCM ensemble is most suitable for regional downscaling. This involves assessing the performance of each GCM in representing the regional circulation systems that influence SA climate in the historical period and the uncertainty in projections in response to anthropogenic forcing. Therefore, this work addresses the following three main questions: (1) how do CMIP6 GCMs represent the most important regional circulation systems in the South America domain; (2) which models project dry and wet scenarios for the precipitation hot spot regions, given the uncertainty in precipitation projections due to the forcing of remote drivers; (3) what is the optimal sub-ensemble of models to represent the circulation in the historical period for each dry and wet scenario.

The paper has the following structure. Sections 2.1 and 2.2 describe the reanalysis and observations, as well as the GCMs used in the analysis. Section 2.3 describes the regional circulation related to the indicators used for validation based on the historical period. Section 2.4 describes the future changes of the main drivers and the storyline approach. Section 3.1 presents the results from the historical period evaluation, followed by the results of precipitation response related to each storyline in Sect. 3.2. The final model selection is reported in Sect. 3.3. Final remarks are presented in Sect. 4.

2 Data and methods

2.1 Reference datasets

The CMIP6 models were validated using the precipitation from the Climatic Research Unit (CRU) observations and the large-scale circulation variables (u and v components of the wind at upper and lower levels, 200 and 850 hPa respectively, and mean sea level pressure) from the European Centre for Medium-Range Weather Forecasts (ECMWF) fifth-generation (ERA5, Hersbach et al. 2020) reanalysis as a reference in the historical evaluation. The CRU Time Series Version 4 (CRU TS4.0) dataset has a monthly temporal resolution, which covers the period from 1901 to 2015. The dataset is based on weather station records (Harris et al. 2020) gridded into a $0.5° \times 0.5°$ degree horizontal resolution (longitude x latitude) grid. The ERA5 reanalysis provides hourly datasets in 137 vertical levels at approximately ~ 31 km horizontal resolution (Hersbach et al. 2020). For this study, we have opted to use monthly datasets, as our main interest is the evaluation of monthly and seasonally large-scale climatological conditions rather than the regional conditions and daily variabilities, since those ones are what the GCMs will pass to the RCM through the boundary conditions. One advantage of using monthly temporal resolution is the availability of a wider range of models. A disadvantage is the smoothing of some regional characteristics, such as those in the SALLJ, which exhibit daily variability, and extratropical cyclones, which are transient events. However, monthly mean precipitation will reflect daily varying moisture-bearing systems. Despite this smoothing, our interest in this work is mainly in the seasonal circulation patterns rather than the daily ones.

2.2 CMIP6 GCM datasets

We used a monthly dataset for 38 models (Table 1, https://aims2.llnl.gov/search) from the Coupled Model Intercomparison Project Phase 6 (CMIP6, Eyring et al. 2016). The variables used to evaluate the historical period and future storylines were precipitation, u and v components of the wind at 850 and 200 hPa, and mean sea level pressure. In the validation step, we used one ensemble member per model, which is referred to in Table 1. Instead, for the storylines, we followed the same approach as outlined in Mindlin et al. (2023), in which we calculated the ensemble mean for each model that shares the same physics. The simulations' quantity and the corresponding ensemble member are reported in Table 1. The climate change analysis was done for the SSP5-8.5 scenario computing the difference between the time slice 2070–2099 and the reference climate (1950–1979) from the historical simulations. The ensemble mean has a better estimate of the climatology by reducing the uncertainty from internal variability when using more members, as shown by Zappa and Shepherd (2017). With this, we consider as many members as possible with the same physics to reduce the uncertainty; however, some models have different numbers of ensemble members, as shown in Table 1.

2.3 Main circulation pattern indicators

As mentioned in the introduction, SAMS and extratropical cyclones are the most important climatological features that modulate the SA circulation and precipitation regime. A set of indicators (Table 2) was elaborated to validate the performance of the GCMs in the historical period (1979–2014) based on the main circulation pattern and precipitation variability that characterise the SA climate in austral summer and winter.

Monsoon circulation systems are formed in response to seasonal changes due to the contrast in temperature between the continent and the ocean (Vera et al. 2006b). Over SA, SAMS characterises the atmospheric circulation and precipitation regime over austral summer (Vera et al. 2006b; Zilli et al. 2018 and 2021; Coelho et al. 2021). The South Atlantic Convergence Zone (SACZ), a diagonally northwestern/southeastern oriented convective band, is a crucial atmospheric feature in austral summer over SA (Kodama 1992 and 1993; Carvalho et al. 2004, Liebmann et al. 2004). This atmospheric system brings precipitation from north to southeastern SA and modulates the SAMS in summertime (Kodama 1992; Jones and Carvalho 2002; Carvalho et al. 2004; Zilli et al. 2017).

Low-level regional circulation during the SAMS season enhances the convective band associated with SACZ events (Kodama 1992 and 1993). For example, moisture and heat are transported by the northeasterly wind, which is part of the western part of the South Atlantic Subtropical High (SASH) and the northwesterly wind known as the South American low-level jet (SALLJ, Marengo et al. 2004). The latter is defined as a northwesterly flux strengthening over the eastern part of the Andes mountains, which contributes to the precipitation in La Plata basin and south/southeastern Brazil (Liebmann et al. 2004; Montini et al. 2019) and modulates the SAMS over the region (Vera et al. 2006b; Montini et al. 2019). Trade winds also cooperate bringing moisture from the tropics to the Amazon basin (Vera et al. 2006b). The subtropical jet stream at upper levels between the subtropical latitudes (30°–35° S) is important for the development of frontogenesis, contributing to convection over the SACZ region (Kodama 1993). Regional circulation at upper levels such as the Bolivian high and northeast

Table 1 CMIP6 GCMs list for each method (validation (V), SL1, SL2 and SL3). Resolutions are shown in degrees (lat × lon) or spectral truncation depending on the model. The number of ensemble members for monthly data available is indicated for the historical and SSP5-8.5 simulations

Models	Institution	N° Runs historical (ssp585) for storyline	Ensemble member of the historical (ssp585) for storyline	Ensemble member for the evaluation	lat/lon grid (°)	Analysis used
ACCESS-CM2	CSIRO	5 (5)	r1:5i1p1f1	r1i1p1f1	1.2 × 1.8	V, SL1, SL2, SL3
ACCESS-ESM1-5		40 (40)	r1:40i1p1f1	r1i1p1f1	1.2 × 1.8	V, SL1, SL2, SL3
BCC-CSM2-MR	Beijing Climate Center, China	3 (1)	r1:3i1p1f1 (r1i1p1f1)	r1i1p1f1	1.1 × 1.1	V, SL1, SL2, SL3
CAMS-CSM1-0	Chinese Academy of Meteorological Sciences, China	2 (2)	r1:2i1p1f1	r1i1p1f1	1.4 × 1.4	V, SL1, SL2, SL3
CanESM5	Canadian Centre for Climate Modeling and Analysis	25 (25)	r1i1p1f1	r1i1p1f1	2.8 × 2.8	V, SL1, SL2, SL3
CAS-ESM2-0	Chinese Academy of Sciences, China	2 (2)	r1-3i1p1f1	r1i1p1f1	1.4 × 1.4	SL2, SL3
CESM2	National Center for Atmospheric Research, Climate and Global Dynamics Laboratory	11 (3)	r1:11i1p1f1 (r4,10,11i1p1f1)	r1i1p1f1	0.9 × 1.25	V, SL1, SL2, SL3
CESM2-WACCM	National Center for Atmospheric Research, Climate and Global Dynamics Laboratory	3 (3)	r1i1p1f1	r1i1p1f1	0.9 × 1.25	V, SL1, SL2, SL3
CIESM	Department of Earth System Science, Tsinghua University	1 (1)	r1i1p1f1	r1i1p1f1	∼1	V, SL2, SL3
CMCC-CM2-SR5	Euro-Mediterranean Center	1 (1)	r1i1p1f1	r1i1p1f1	∼1	V, SL1, SL2, SL3
CMCC-EM2		1 (1)	r1i1p1f1	r1i1p1f1	0.9 × 1.25	V, SL2, SL3
CNRM-CM6-1	National Center of Meteorological Research (NCMR), France	30 (6)	r1i1p1f2	r1i1p1f2	T359	V, SL1, SL2, SL3
CNRM-ESM2-1		10 (5)	r1i1p1f2	r1i1p1f2	T359	V, SL1, SL2, SL3
E3SM-1–0	Lawrence Livermore National Laboratory and collaborators, USA	5 (4)	r1:5i1p1f1 (r1-2,3-5i1p1f1)	r1i1p1f1	1 × 4	V, SL2, SL3
EC-Earth3	EC-EARTH consortium, The Netherlands/Ireland	1 (1)	r1i1p1f1	r1i1p1f1	0.7 × 0.7	V, SL1, SL2, SL3
FGOALS-g3	Chinese Academy of Sciences, China	6 (4)	r1i1p1f1	r1i1p1f1	2.0 × 2.3	V, SL1, SL2, SL3
FIO-ESM-2–0	First Institute of Oceanography, State Oceanic Administration, China	3 (3)	r1:3i1p1f1	r1i1p1f1	0.9 × 1.25	V, SL2, SL3
GFDL-CM4	National Oceanic and Atmospheric Administration, USA	1 (1)	r1i1p1f1	r1i1p1f1	∼1	V, SL2, SL3
GISS-E2-1-G	NASA Goddard Institute for Space Studies, New York, USA		r1:11i1p1f1 (r1:4i1p1f1)	r1i1p1f2	2 × 2.5	V, SL2, SL3
GISS-E2-1-H			r1:5i1p1f1 (r1:5i1p1f1)	r1i1p1f2	2 × 2.5	V, SL2, SL3
HadGEM3-GC31-LL	UK Met Office Hadley Center, UK	4 (4)	r1:4i1p1f1	r3i1p1f1	2.2 × 2.2	V, SL1, SL2, SL3
HadGEM3-GC31-MM		4 (4)	r1:4i1p1f1	r3i1p1f1	0.9 × 0.9	V, SL1, SL2, SL3
IITM-ESM	Centre for Climate Change Research, Indian Institute of Tropical Meteorology Pune	1 (1)	r1i1p1f1	r1i1p1f1	0.95 × 1.87	V, SL1, SL2, SL3
INM-CM4-8	Institute for Numerical Mathematics (INM), Russia	1 (1)	r1i1p1f1	r1i1p1f1	1.5 × 2.0	V, SL1, SL2, SL3
INM-CM5-0		10 (1)	r1i1p1f1	r1i1p1f1	1.5 × 2.0	V, SL1, SL2, SL3
IPSL-CM6A-LR	Institute Pierre Simon Laplace, France	33 (6)	r1:33i1p1f1 (r1:4,6,33i1p1f1)	r1i1p1f1	1.25 × 2.5	V, SL2, SL3
KACE-1–0-G	Nat. Inst. of Meteorological Sciences/Korea Meteorological Admin	3 (3)	r1i1p1f1	r1i1p1f1	2.2 × 2.2	V, SL1, SL2, SL3
MIROC6	National Institute for Environmental Studies, Japan	50 (50)	r1:50i1p1f1	r1i1p1f1	1.4 × 1.4	V, SL1, SL2, SL3
MIROC-ES2L		30 (10)	r1:30i1p1f2 (r1:10i1p1f2)	r1i1p1f2	4.5 × 4.5	V, SL1, SL2, SL3
MCM-UA-1–0	University of Arizona, USA	1 (1)	r1i1p1f2	r1i1p1f2	3.75 × 2.5	V, SL2, SL3

Table 1 (continued)

Models	Institution	N° Runs historical (ssp585) for storyline	Ensemble member of the historical (ssp585) for storyline	Ensemble member for the evaluation	lat/lon grid (°)	Analysis used
MPI-ESM1-2-HR	Max Planck Institute for Meteorology (MPI), Germany	10 (10)	r1i1p1f1	r1i1p1f1	~0.9	V, SL1, SL2, SL3
MPI-ESM1-2-LR		30 (10)	r1i1p1f1	r1i1p1f1	~2.0	V, SL1, SL2, SL3
MRI-ESM2-0	Meteorological Research Institute, Japan	10 (5)	r1:10i1p1f1 (r1:5i1p1f1)	r1i1p1f1	1.1 × 1.1	V, SL1, SL2, SL3
NESM3	Nanjing University of Information Science and Technology	5 (2)	r1:5i1p1f1 (r1:2i1p1f1)	r1i1p1f1	1.9 × 1.9	V, SL1, SL2, SL3
NorESM2-LM	Norwegian Climate Center, Norway	3 (1)	r1:3i1p1f1 (r1i1p1f1)	r1i1p1f1	1.9 × 2.5	V, SL1, SL2, SL3
NorESM2-MM		3 (1)	r1:3i1p1f1 (r1i1p1f1)	r1i1p1f1	0.9 × 0.9	V, SL1, SL2, SL3
UKESM1-0-LL	UK Met Office and NERC research centers	19 (5)	r1:19i1p1f2 (r1:4,8i1p1f2)	r1i1p1f2	1.3 × 1.9	V, SL1, SL2, SL3
TaiESM1	Taiwan Earth System Model	2 (1)	r1:2i1p1f1 (r1i1p1f1)	r1i1p1f1	0.9 × 0.9	V, SL1, SL2, SL3

* V, Validation; SL1, Storyline 1; SL2, Storyline 2; SL3, Storyline 3

trough enhance the circulation pattern at low levels, which contributes to the precipitation over the SAMS region.

In order to assess the precipitation patterns associated with SACZ events and SAMS season, three indicators have been defined (from 1 to 3 in Table 2) focusing on three specific regions: the Amazon Basin, the La Plata Basin, and Southeastern Brazil as shown in Fig. 1.

The first indicator was chosen to represent the temporal and spatial variability in the annual cycle of precipitation over the Amazon Basin. A Hovmoller diagram has been used to represent the averaged precipitation along the longitude range 65°–50° W and the latitude range 0–15°S for the Amazon basin box for each month of the year for the CRU TS4.0 observational dataset (see details in Table 2 and Fig. 2a). Indicator 2 represents the annual cycle of precipitation as shown in Fig. 3 over the three regions: Amazon basin (AMZ), Southeastern coast of Brazil (SESA-F, Zilli et al. 2018), and La Plata basin (LPB), as highlighted in Fig. 1. Indicator 3 represents the DJF mean precipitation pattern in the same three regions as above. Further details are reported in Table 2.

The upper- and low- level circulation indicators were developed to assess the physical circulations that contribute to the development of the SACZ, SALLJ and polar jet stream features as described above. To validate these circulations for the downscaling approach, these features must be accurately represented in terms of their spatial patterns, as GCMs provide the large-scale signatures used in the boundary conditions for RCMs. Thus, to build the indicators, we considered the climatological positions of the systems considering relevant variables that describe them in terms of wind speed and mean sea level pressure. These positions were identified using ERA5 as a reference. Based on the systems' identified positions for wind speed and mean sea level pressure, the indicators evaluate the spatial correlation between the model climatology and the ERA5 climatology for each season.

An overview of the spatial fields for wind speed at 850 hPa and 200 hPa, and mean sea level pressure for the austral summer and winter for ERA5, is shown in Fig. 4. The wind speed fields at 850 hPa for both seasons are shown in Fig. 4a and b. The maximum wind speed is observed near Bolivia, indicating the characteristics of the SALLJ pattern, which is more pronounced in winter and can be associated with the more intense trade winds in this season. In winter, the position of SASH is located further north and elongated towards the continent more than in summer (Fig. 4a, b). The upper-level jets are indicated in the wind speed field at 200 hPa (Fig. 4c, d), being more intense and closer to the continent in winter (Fig. 4d).

The spatial correlation of the climatological upper- and low- level circulation system positions allows us to quantify the model accuracy; if the GCMs do not represent the regional circulation structure the correlation values are small (less than 0.5). Higher correlation values mean that GCMs have a good representation of the low- and upper-level circulation positions, and consequently, GCMs can be trustworthy when used for downscaling purposes in a specific domain.

The circulation indicators are from 4 to 9, with the austral summer (DJF) between 4 and 6, and winter (JJA) from 7 to 9. Indicator 4 was chosen to capture the spatial variability of the semi permanent high pressure signature over SA known as SASH and South Pacific Subtropical High. The indicator calculates the spatial correlation of the high-pressure core positions (15°–32° W; 2°N–40°S and 78°–110° W; 15°–45°

Table 2 Description of the validation indicators

Climatological circulation	Index number	Variables	Period	Method
South America Monsoon	1	Precipitation	Annual	Spatial correlation of the Hovmoller diagram precipitation patterns in a fixed longitude (65°–50° W) and variation of latitude (0–15° S) in the Amazon basin region between CRU and CMIP6 GCMs
	2		DJF	Spatial correlation of the seasonal precipitation pattern in the three regions (Amazon basin—50°–65° W and 0°–15° S, Southeastern Brazil—40°–49° W; 20°–25° S, and La Plata basin—49°–62° W; 20°–32°S, Fig. 1) between CRU and CMIP6 GCMs
	3		Annual	Temporal correlation of the averaged precipitation annual cycle in three regions (Amazon basin—50°–65° W and 0°–15° S, Southeastern Brazil—40°–49° W; 20°–25° S, and La Plata basin—49°–62° W; 20°–32°S, Fig. 3) between CRU and each model
South American Monsoon and extratropical cyclones	4	Sea level pressure	DJF	Spatial correlation of the mean sea level pressure for the SASH (15°–32° W; 2°N–40°S) and South Pacific Subtropical High (78°–110° W; 15°–45°S) positions as a schematic illustration in Fig. 4a (contours) between ERA5 and each GCMs CMIP6
	5	Wind speed at 850 hPa		Spatial correlation of the wind speed at 850 hPa for SALLJ northwestern-southeastern direction band position (top left and right end are in 77° W–9° S and 62° W–10° S and the bottom are 45° W–25° S and 62° W and 27° S), and trade winds (17°–73° W; 2° N–12° S) position as illustrated in shaded by Fig. 4a between ERA5 and CMIP6 GCMs
	6	Wind speed at 200 hPa		Spatial correlation of the wind speed at 200 hPa for the upper-level jet stream (80° W–10° E; 27°–53° S), Bolivian high (82°–57° W; 2°–25°), and northeast trough (42°–18°; 2° N–25° S) positions as illustrated in Fig. 4c between ERA5 and CMIP6 GCMs
Extratropical cyclones	7	Sea level pressure	JJA	Spatial correlation of the mean sea level pressure in the SASH (32° W–2° E; 15°–40° S) and South Pacific Subtropical High (110°–78° W; 15°–42° S) positions as illustrated in Fig. 4b (contours) between ERA5 and CMIP6 GCMs
	8	Wind speed at 850		Spatial correlation between ERA5 and each model in the SALLL's position in a northwestern-southeastern band (top left and right end are in 70° W–15° S and 62° W–9° S and the bottom are 43° W–28° S and 53° W and 38° S) and trade winds position (62°–28° W; 2° N–8°S) as illustrated shaded in Fig. 4b
	9	Wind speed at 200 hPa		Spatial correlation of the wind at 200 hPa in the upper-level jet stream position (82°W–2° E; 18°–48° S) as illustrated in Fig. 4d between ERA5 and each model

* SALLJ, South American Low-Level Jet; SACZ, South Atlantic Convergence Zone; SASH, South Atlantic Subtropical High; SAMS, South American Monsoon System

S) in DJF as illustrated in Fig. 4a (contours). As explained, physically, the SASH impacts the SAMS and extratropical cyclones by transporting warm and moist air from the ocean to the continent. In order to assess the GCMs' representation of the spatial variability of the SALLJ and trade winds as the main circulation that impacts the SAMS in DJF as explained before, indicator 5 measures the spatial correlation for the position of both features in the wind speed at 850 hPa. SALLJ position was chosen to capture the maximum core extension, which is in a northwest-southeastern orientation (top left and right end are 77° W–9° S and 62° W-10° S, and the bottom are 45° W–25° S and 62° W and 27° S) and for the trade winds the position is 17°–73° W, 2° N–12° S as illustrated in Fig. 4a. At the upper level, the features that impact the SAMS and extratropical cyclones' configuration are the jet stream, Bolivian high, and northeast trough. With that, indicator 6 was chosen to capture the system configuration positions, especially the jet stream core. The calculation is based on the spatial correlation represented by the wind speed at 200 hPa as illustrated in Fig. 4c.

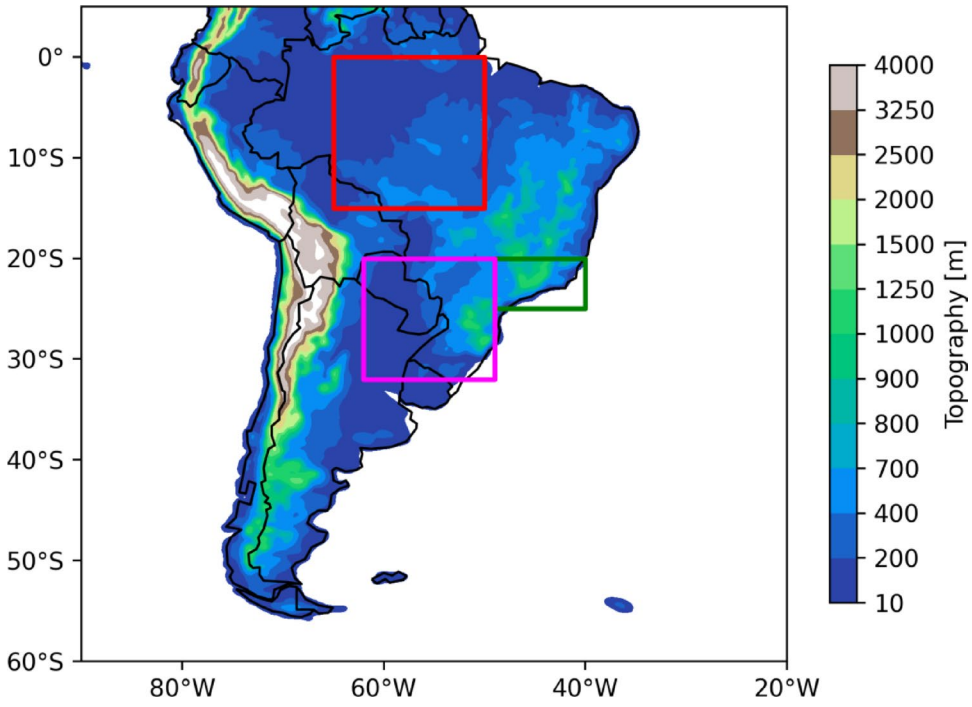

Fig. 1 Topographic elevation in meters in the South American domain with three highlighted regions: the Amazon (red, 50°–65° W and 0°–15° S), La Plata basin (pink, 49°–62° W; 20°–32°S) and SESA-F (green, 40°–49° W; 20°–25° S; Zilli et al. 2018)

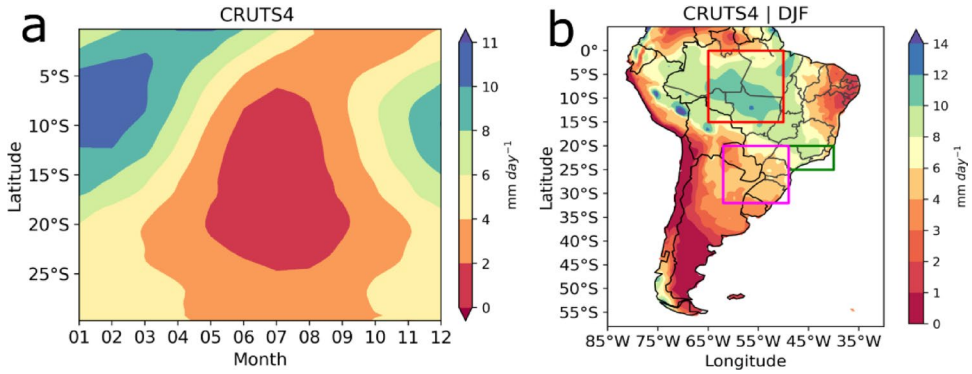

Fig. 2 Examples of the precipitation metrics used in indicators 1–3 for the CRU as a reference. **a** Hovmoller diagram and **b** austral summer (DJF) mean precipitation. The boxes highlighted in b are as in Fig. 1

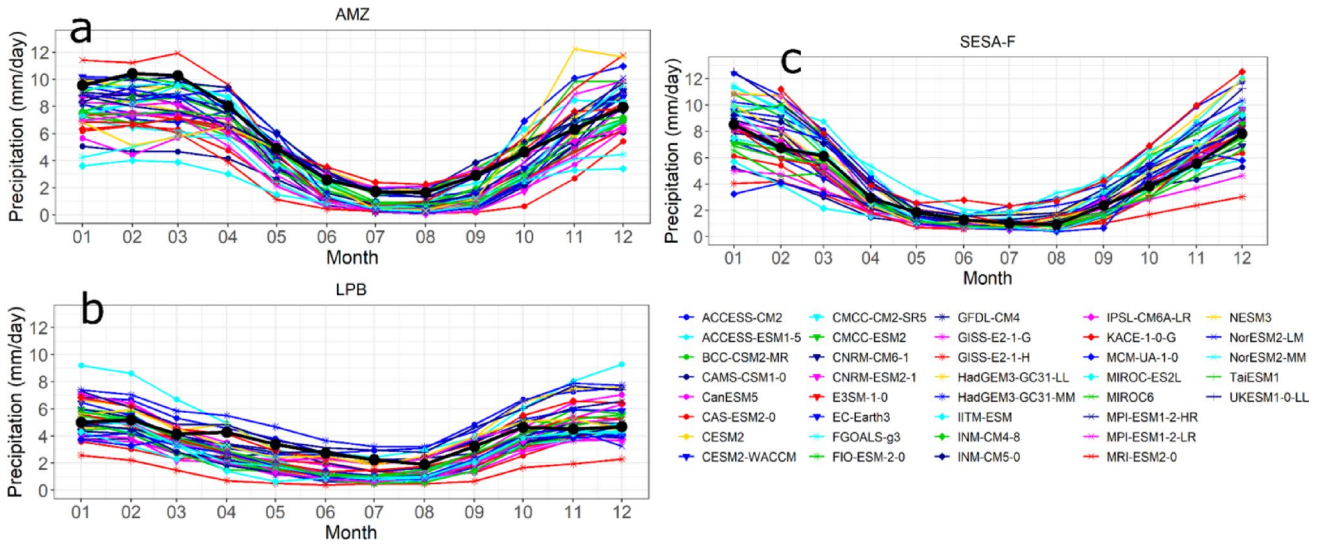

Fig. 3 Mean precipitation annual cycle for the historical period (1979–2014) in 38 models (colour lines) and CRU (bold black line) for: **a** Amazon basin, **b** La Plata basin and **c** SESA-F

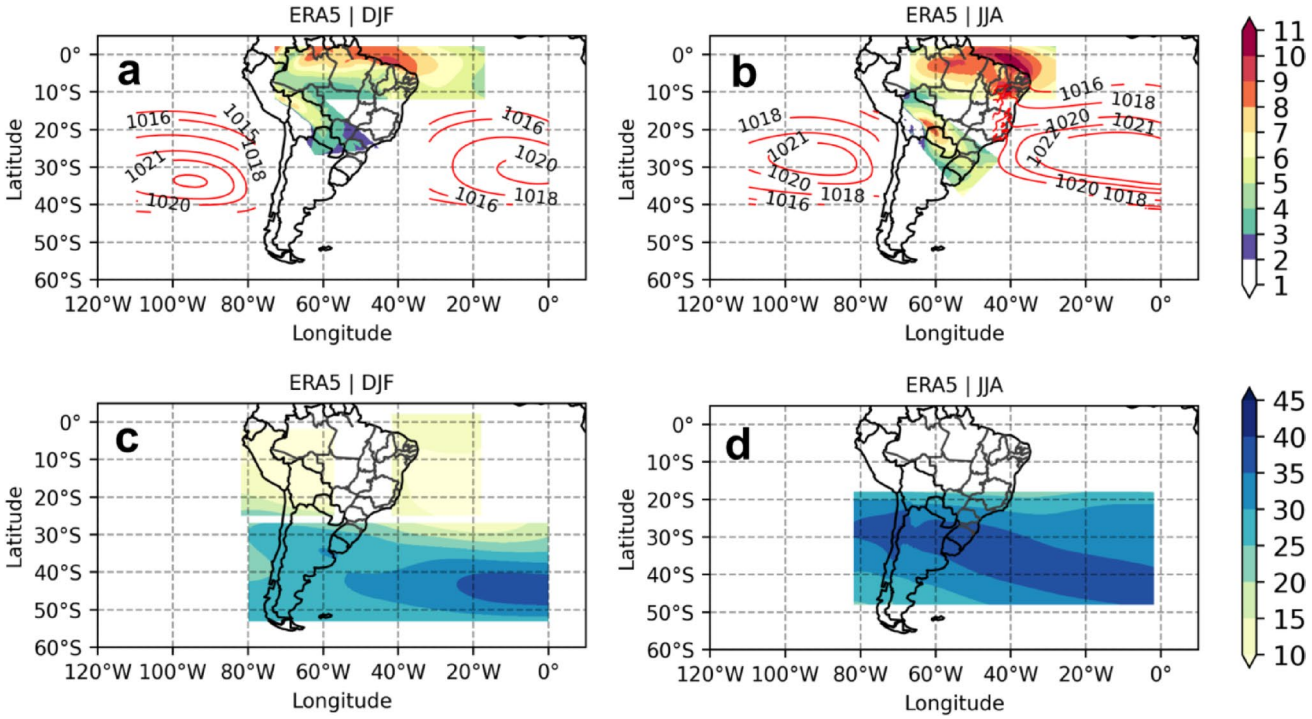

Fig. 4 Climatological positions of the low- and upper-level circulation fields for ERA5 in Austral summer (DJF) and winter (JJA). Low-level wind speed at 850 hPa (shaded, m s^{-1}) and mean sea level pressure (contours, hPa) are shown in panels (**a**) and (**b**), and upper-level wind speed at 200 hPa (shaded, m s^{-1}) is shown in panels (**c**) and (**d**), for summer (DJF) and winter (JJA) respectively

In austral winter and summer, extratropical cyclones impact the east coast of SA, which affects coastal cities with high precipitation accumulations, wind gusts, and storm surges (da Rocha et al. 2004; Mindlin et al. 2020; Cardoso et al. 2022). Three main cyclogenetic regions are very well documented on the east coast of SA (Hoskins and Hodges 2005; Reboita et al. 2010a; Gramcianinov et al. 2019; Crespo et al. 2020), and we are interested in the Uruguay/La Plata basin region and the southeastern coast of Brazil given its impact on the precipitation variability in SA. Cyclogenesis in these two regions is mostly driven by the moisture and heat transport from the SASH over the southeastern coast of Brazil (Mendes et al. 2009; Gramcianinov et al. 2019; Cardoso et al. 2022), while in La Plata region moist and warm air transport comes from the SALLJ. Another circulation feature that impacts the cyclogenesis in the region is the subtropical jet for the southeastern coast of Brazil and the polar jet for Uruguay/La Plata (Gramcianinov et al. 2019; Crespo et al. 2020; De Jesus et al. 2020).

The precipitation patterns in both regions (LPB and SESA-F) have already been represented in indicators 2 and 3, which consider austral summer (DJF) and the annual cycle, respectively. For the winter climatological regional circulation, we used similar indicators as for summer ones, changing the positions accordingly with the season. The indicators from 7 to 9 summarise the spatial variability of the climatological patterns influencing extratropical cyclones in SESA-F and LPB in JJA based on the spatial correlation positions of each system. Indicator 7, as indicator 4, measures the SASH and South Pacific Subtropical High position. In the same way as for the DJF indicator, indicator 8 measures the trade wind and SALLJ position spatial correlation in JJA as illustrated in Fig. 4c. Different from DJF, the upper level features that impact the extratropical cyclones in JJA are only the upper level jet, thus indicator 9 captures the spatial variability of the jet stream position as illustrated in Fig. 4d.

2.4 Storyline approach to account for regional circulation uncertainty

2.4.1 Main driver definitions

The spread in multimodel ensembles can be described, at least in part, with a small set of indices that capture the uncertainty in the response of the most relevant atmospheric circulation patterns, here referred to as main drivers (Manzini et al. 2014; Zappa and Shepherd 2017; Mindlin et al. 2020 and 2023).

In this work, the indices (detailed in Table 3) were chosen to represent the main drivers for SA precipitation uncertainty based on the main circulation systems that modulate the precipitation regime, such as extratropical cyclone changes in DJF (storyline set 1), for which we considered

Table 3 Definition of the indices of the main drivers for the three storylines

Storylines	Season	Index	Description
SL1	DJF	Tropical upper-tropospheric warming (ΔT_{trop})	Change in temperature at 250 hPa zonally averaged between 15° S and 15° N (Mindlin et al. 2020)
SL1	DJF	Stratospheric vortex breakdown delay (Δ_{VB})	Difference between the climatological vortex breakdown in Julian days in the future projections and the breakdown date in the historical period (Mindlin et al. 2020)
SL1	DJF	Central Pacific asymmetric sea surface temperature change (ΔCPasym)	Temperature changes averaged over the box of 5° N–5° S and 180° E–110° W (Mindlin et al. 2023)
SL1	DJF	Eastern Pacific asymmetric sea surface temperature change (ΔEPasym)	Temperature changes averaged over the box of 0° N–10° S and 90°–80° W (Mindlin et al. 2023)
SL2	DJF	SACZ Position shift ($\Delta_{SACZ\text{-}shift}$)	The precipitation position band is calculated by applying a linear regression with longitude as the independent variable and the latitude of the precipitation maximum as the dependent variable. The index is the changes, i.e., the difference between the position of future projections and the historical period
SL2	DJF	SALLJ strengthening changes ($\Delta_{SALLJ\text{-}DJF}$)	The difference between the future projections and historical period for the wind speed at 850 hPa in the SALLJ position averaged area in a northwestern-southeastern direction band (top left and right end are 77° W–9° S and 62° W–10° S and the bottom are 45° W–25° S and 62° W and 27° S) as shown in shading in Fig. 4a
SL3	JJA	SALLJ strengthening changes ($\Delta_{SALLJ\text{-}JJA}$)	The difference between the future projections and the historical period for the wind speed at 850 hPa in the averaged box of the SALLJ position averaged area (top left and right end are in 70° W–15° S and 62° W–9° S and the bottom are 43° W–28° S and 53° W and 38° S) as displayed in Fig. 4b
SL3	JJA	Polar jet strengthening ($\Delta_{polar\text{-}JJA}$)	The index evaluates the wind speed at 200 hPa changes (difference between future projections and historical period) in an averaged area of 82°W–2° E; 18°–48° S as illustrated in Fig. 4d

* SALLJ, South American Low-Level Jet; SACZ, South Atlantic Convergence Zone; SASH, South Atlantic Subtropical High

the results from Mindlin et al. (2023) for this storyline set. The two other storyline sets are for the SAMS changes in DJF (storyline set 2) and extratropical cyclone changes in JJA (storyline set 3). Here, we used the storyline set terminology to represent the different sets of main drivers that explain a large-scale choice and different seasons.

In the first storyline set (SL1), we use previous work results by Mindlin et al. (2023), who considered large-scale circulation as the driver of uncertainty (index calculations detailed in Table 3). In SL1, the changes are controlled by the zonally symmetric upper tropospheric tropical warming, the seasonal extension of the stratospheric polar vortex (which is represented by the delayed vortex breakdown date), and asymmetric sea surface temperature warming patterns. Forced responses in these drivers lead to changes in the extratropical cyclones' intensity and position and Hadley cell expansion, consequently influencing precipitation regimes and circulation changes over the Southeastern South America region. For more details, we refer to Mindlin et al. (2023).

The second and third storyline sets, referred to as SL2 and SL3, were developed to analyse regional circulation uncertainty considering the main drivers that control SAMS changes (DJF, SL2) and extratropical cyclones (JJA, SL3). These drivers are the SACZ and SALLJ for SL2 and SALLJ and the polar jet for SL3. The selection of these drivers and the definition of indices to capture their changes was done based on a detailed literature review, presented in the following paragraphs.

A poleward shift in SACZ events has been observed in the historical periods in both observational datasets (Zilli et al. 2018) and GCMs (Zilli et al. 2021), mainly because of a change in the SASH position and intensity (Zilli et al. 2018). The tropical tropospheric warming induces the southward Hadley cell expansion and poleward shift of westerly winds (Butler et al. 2010; Schmidt and Grise 2017), contributing to the southwestward shift of SASH (Zilli et al. 2018; Reboita

et al. 2019). We create an index to represent the SACZ position changes based on the precipitation band (Table 3) by applying a spatial linear regression model as in Narsey et al. (2022). SALLJ, the second main driver that impacts SAMS features, shows a strengthening in SALLJ features in GCM and RCM projections (Soares and Marengo 2008; Torres-Alavez et al. 2021). Projections show a westward SALLJ expansion (Torres-Alavez et al. 2021) at the end of the century with the RCP8.5 scenario. Therefore, we describe the SALLJ strengthening changes based on the wind speed at 850 hPa as a measure of the intensity (detailed in Table 3).

With the third storyline set (SL3), we aim to assess the changes related to extratropical cyclones in the austral winter (JJA) based on the changes in two main drivers. Extratropical cyclones are impacted mostly by moisture and heat transport by SALLJ, and the polar jet features as already explained in the section above. The strengthening of SALLJ throughout the year in response to anthropogenic forcing was reported by Soares and Marengo (2008). To quantify SALLJ changes, we defined a similar index as for DJF (Table 3). The strengthening and poleward shift of the polar jets in JJA in response to anthropogenic forcing was reported by many studies (Lu et al. 2007; Rivière 2011; de Jesus et al. 2020; Mindlin et al. 2020; Gulev et al. 2021), and the uncertainty in this circulation response can explain a significant fraction of the spread in the precipitation response in southeastern SA during JJA (Mindlin et al. 2020). Thus, we consider the polar jet change in intensity and position as the second driver in JJA (Table 3).

2.4.2 Linear regression and storyline frameworks

The storyline approach is used to define different plausible futures considering SAMS and extratropical cyclone changes in response to greenhouse gas forcing. For that, the indices (Table 3) of each remote and proximate driver's changes explained above are used as covariates in a multiple linear regression framework. The linear regression framework is used to evaluate the circulation and precipitation response and quantify the precipitation sensitivity to the uncertainty of the main drivers' response (Zappa and Shepherd 2017; Mindlin et al. 2020 and 2023). The linear statistical models used in this work are detailed in Appendix A.

In more detail, the storyline assessment aims to interpret the precipitation spread in a model ensemble based on the spread of a small set of indices that capture the key atmospheric circulation responses relevant for precipitation over SA. Each index represents a large-scale driver, such as changes in the SACZ, SALLJ, or the polar jet. For each climate model, the response of precipitation and circulation variables is computed as the difference between a future period and a reference climatology, and then divided by the model's global-mean warming. This step removes differences in climate sensitivity across models and isolates the spatial pattern of the forced response. Similarly, the circulation indices used as predictors are also scaled by global warming. In this way, both predictors and responses are expressed per degree of global warming, so that the regression analysis targets the inter-model spread in the spatial pattern of change rather than in the magnitude of warming.

We then apply a multiple linear regression framework in which the scaled precipitation response of each model for every grid-cell is expressed as a linear combination of the scaled indices representing the main circulation drivers. The regression coefficients quantify the sensitivity of precipitation change to each driver, interpreted as the additional precipitation change per degree of warming that a model projects if its circulation response in that driver is one standard deviation larger than the ensemble mean. This approach provides a statistical estimate of the link between large-scale circulation responses and regional precipitation outcomes, attributing part of the inter-model spread to physically interpretable drivers.

Finally, the regression framework is used to construct storylines, which are self-consistent combinations of driver responses designed to span the plausible range of outcomes within the model ensemble. For each storyline, the precipitation change is expressed as the sum of the ensemble-mean response per degree of global warming, and the linear contributions of each driver. These contributions are obtained by multiplying the regression coefficients by the deviation of the driver from its ensemble mean. In other words, the storyline quantifies how much wetter or drier the climate becomes when the circulation response departs from the mean by a specified standardized amount. In the previous literature, this standardized departure has been referred to as the "storyline coefficient", highlighting its role as the key parameter that characterizes each storyline. The selection of storylines aims to represent the extremes of possible circulation futures, while still ensuring plausibility. To achieve this, we restrict the choices to lie within the 80% confidence region of the joint distribution of the driver responses (indicated by the ellipse or circle in Fig. 5), which correspond to a storyline coefficient of 1.26 standard deviation in both drivers (Zappa and Shepherd 2017). Figure 5 shows the ensemble spread in the drivers used in each storyline set and the 80% confidence region. The 80% confidence region selection generates plausible yet extreme storylines, following Zappa and Shepherd (2017). Mindlin et al. (2023) instead conditioned storylines on extreme wet and dry responses, rather than prescribing a confidence region for the drivers (Fig. 11 from Mindlin et al. (2023)). Their results show that the associated remote driver responses still fall within the 70–90% confidence range, with the precise level depending

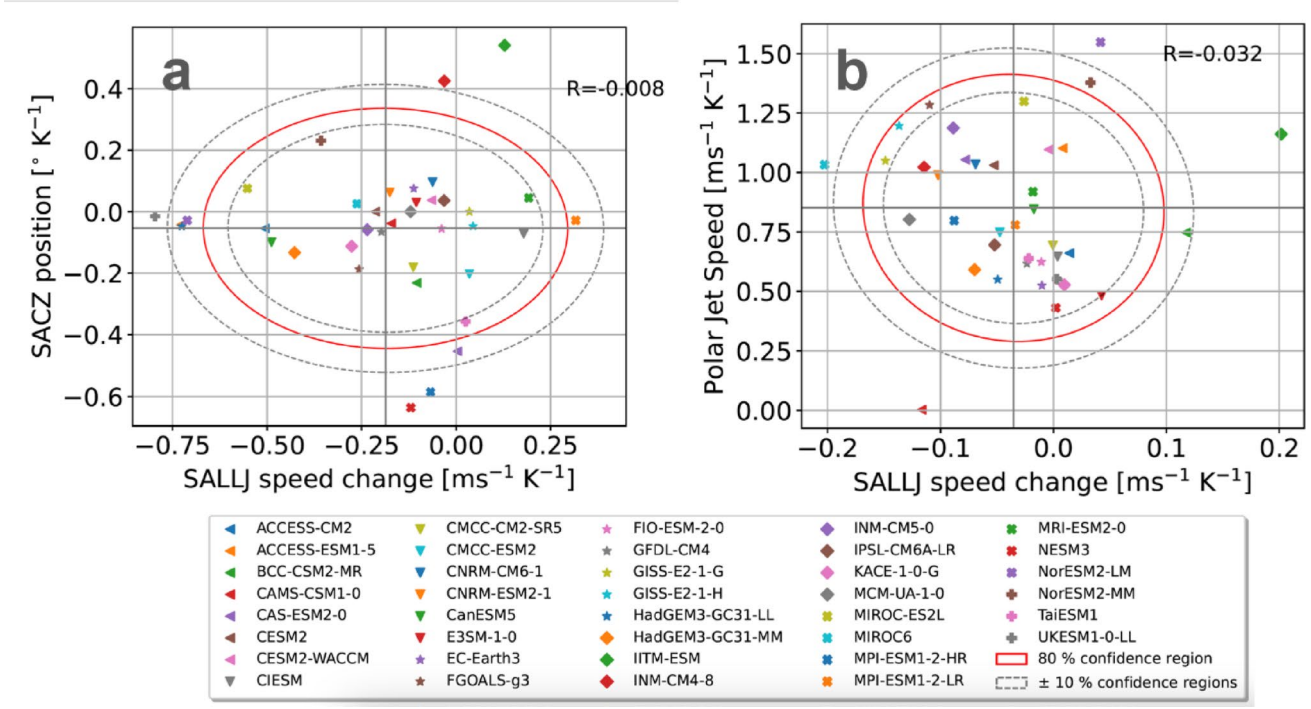

Fig. 5 CMIP6 model responses in **a** SACZ shift and SALLJ speed change in DJF (SL2) and **b** polar jet speed and SALLJ speed change in JJA (SL3). The red curve shows the 80% confidence ellipse of the joint distribution with two degrees of freedom

on the region. Since the relevance of remote drivers varies regionally, they conclude that an 80% confidence region provides a consistent representation of extreme yet plausible precipitation responses based on a reduced set of drivers that explain part of the model variance.

The summer storyline set (SL2) is developed based on an equatorward/poleward shift of the SACZ and a weakening/strengthening of SALLJ (Fig. 5a). The winter storyline set is developed based on polar jet speed and SALLJ speed change in JJA (Fig. 5b). By sampling these phase spaces, we generate four storylines per season that describe contrasting but plausible circulation regimes. These regimes can then be used to evaluate the associated precipitation responses and to select a sub-ensemble of models that represents both the mean state and the range of plausible futures. Although many models project, for example, a poleward SACZ shift or a strengthening of the SALLJ, some show the opposite response. The storyline approach thus highlights the spread among models and provides a structured way of ensuring that the downscaling ensemble captures both the wettest and driest plausible futures.

The precipitation response in each model can be controlled by regional and local factors other than the proposed circulation patterns, some of which could even be related to misrepresentations of local processes in GCMs. To inform the model selection we estimated the precipitation response controlled only by the proposed drivers in the three regions (SESA-F (SL1), Amazon basin (SL2) and La Plata basin (SL3)) as a linear combination of the MEM and the sensitivity to the main drivers multiplied by the standardised value of the remote driver index in each model. This provides a summary of the precipitation spread captured by the circulation storylines and allows the identification of the wet and dry responses for each region, which enables the selection of a group of models for downscaling.

3 Results

3.1 Historical validation of regional circulation

Indicators were created to represent the most important circulation and precipitation patterns over SA based on a representative set of variables (explained in Sect. 2.3). They summarise whether each model accurately represents SA climate in the historical period. Their evaluation is presented in Fig. 6. Indicators 1 to 3 represent precipitation patterns in the AMZ, the LPB and SESA-F. Indicators 4 to 9 describe the main low- and upper-level climatological circulation patterns over the SA.

In general terms, CMIP6 GCMs have difficulty representing local processes and topography, which leads to difficulties in accurately representing the precipitation regime in austral summer over SA (Sun et al. 2006; Dai 2006; Vera

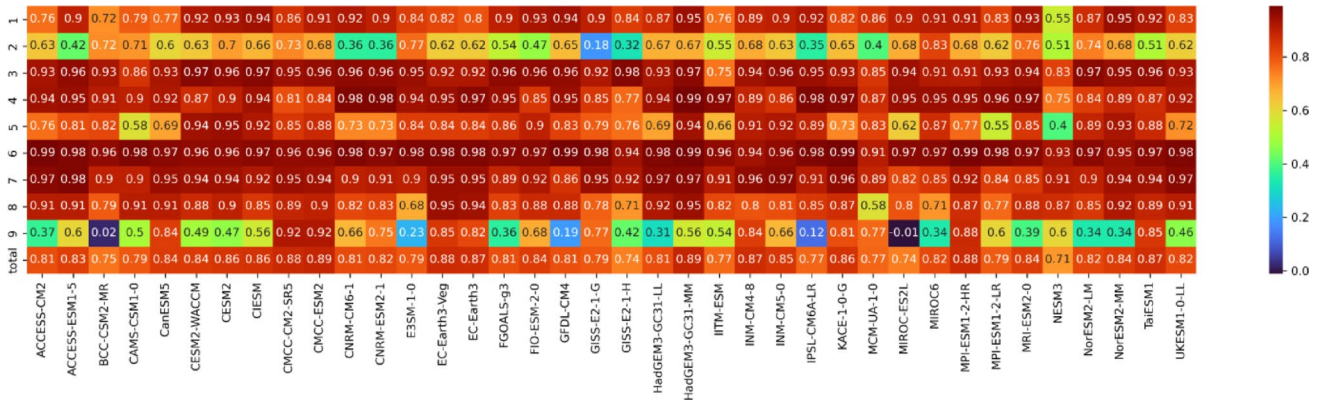

Fig. 6 Heatmap for the correlation values of the 9 indicators and the total score (y axis) and 38 GCMs (x axis) for the period 1979–2014

et al. 2006b; Bombardi and Carvalho 2009; Llopart et al. 2014). Most models (12 of the 38 total) present a precipitation spatial correlation for DJF (indicator 2) lower than 0.5; only 7 GCMs exceed values of 0.7. MIROC6 has the best performance with a correlation coefficient of 0.83, while GISS-E2-1-G has the worst performance with a correlation of 0.18. On the other hand, the spatial and temporal correlation values for the annual cycle for the Amazon basin (indicator 1) and the three regions together (indicator 3) are high. Indicator 1 records the lowest correlation of 0.55 in NESM3, but overall models show good performance (>0.75) with the highest being 0.95 in NorESM2-MM. CMIP6 GCMs show good performance when simulating the annual cycle phase in all three regions (indicator 3, Fig. 3), i.e., they capture the low precipitation regime from May to September, and high regime from October to April, which is reflected in the high correlation (>0.8).

GCMs perform well (correlation greater than>0.8) in representing the semi-stationary pressure patterns captured by indicator 4. The circulation patterns of SALLJ and trade winds are captured by indicator 5, which considers the wind speed at 850 hPa. Some models have difficulty in representing these patterns. The NESM3 model presents correlations of 0.4, while the highest correlations are with the CESM2 and CESM2-WACCM models with 0.95 and 0.94. SALLJ is influenced by the Andes Mountains (Vera et al. 2006b), reflecting the lower spatial correlation in representing the system position among some models. Models with lower correlations (NESM3 and MPI-ESM3-LR) also have lower scores in precipitation indicators. SALLJ significantly influences the precipitation regime over the La Plata basin and the Amazon (Vera et al. 2006a, b; Jones 2019). Indicator 6 represents the high-level patterns for the Austral summer (jet streams, Bolivian high and northeast trough as already discussed). All models have spatial correlations larger than 0.9.

As winter is the dry season over SA (Reboita et al. 2010b; Coelho et al. 2021; Ferreira and Reboita 2022), only the circulation patterns were analysed. In general terms, GCMs represent very well the JJA position of the semi-stationary pressure high over the South Atlantic and Pacific Oceans as was already observed in DJF. GCMs have a better performance in representing the SALLJ in winter than in summer (indicator 8). At upper levels, all models have difficulties simulating the jet stream position, with most models showing a spatial correlation lower than 0.5 (16 of 38 models). The jet stream at upper levels in austral winter has a large contribution to extratropical cyclogenesis over La Plata/Uruguay and the southeastern coast of Brazil (Reboita et al. 2012; Gramcianinov et al. 2019; Crespo et al. 2020; de Jesus et al. 2020). The misrepresentation of jet streams in winter can result in cyclone frequency errors, and consequently precipitation errors.

Other works developed a different approach to validate the CMIP6 GCM models. For instance, Olmo et al. (2022) conducted a GCMs validation for the circulation patterns at low levels and precipitation with 16 GCMs over South Tropical SA. Their results show that the CESM2, CMCC-CM2-HR4 and MPI-ESM1-2-HR models have a good performance in representing six different types of circulation patterns and seasons. However, they also show that CanESM5 and NorESM2-MM models have good performance in representing low-level circulation, precipitation and other levels of circulation compared to ERA5. Here, we apply different indices and methodology and we end up having some overlapping in the final model selection. Arias et al. (2025) conducted another study focusing on the boundary regions of regional downscaling and large circulations features. They showed that the most suitable model can vary among the indices being used.

3.2 Circulation and precipitation response to remote drivers and dynamical storylines of future changes

This section provides an overview of the precipitation and circulation response considering the combinations of the main driver responses defined in Sect. 2.4 for the three storyline sets. This combination is calculated using the methodology described in Zappa and Shepherd (2017) and summarised in the storyline phase diagram (Fig. 5). These analyses are important to understand the circulation and precipitation response of the combination of extremes of the main drivers for each storyline, and to assess that the selection based on the proposed drivers is representative of the different plausible futures in each region of interest.

A summary of the circulation and precipitation response for SL1 is summarised here; for more details the reader is referred to Mindlin et al. (2023). The drying associated with the precipitation response in the storyline over SESA-F is associated with a high upper-tropospheric tropical warming, an early stratospheric polar vortex breakdown date and a weak warming of the tropical Pacific sea surface temperature. In contrast, the wetting response is associated with a low upper-tropospheric tropical warming, a late stratospheric polar vortex breakdown date and a strong warming of the tropical Pacific sea surface temperature. Although there are more models representing a wetting storyline, the agreement could be related to model dependence and is no guarantee of a more probable response.

For SL2 and SL3, the precipitation responses for the AMZ and LPB in DJF and JJA are shown in Fig. 7. Each field shows the regional response under a particular combination of extreme remote driver responses (Fig. 5) estimated with the linear regression.

Figure 7a shows the precipitation response for SL2 (extreme combinations of SACZ and SALLJ responses), in which the negative index means poleward (negative latitude change) and the positive index is more equatorward (positive latitude change). The combination of an equatorward SACZ shift (positive change) and a high (low) SALLJ strengthening leads to a wet (dry) response over the Amazon basin. On the other hand, the other three combinations show a general dry condition in the Amazon basin. Even with an equatorward shift, the precipitation response combined with a SALLJ weakening remains dry, highlighting the SALLJ's crucial role in the Amazon basin precipitation pattern. In the

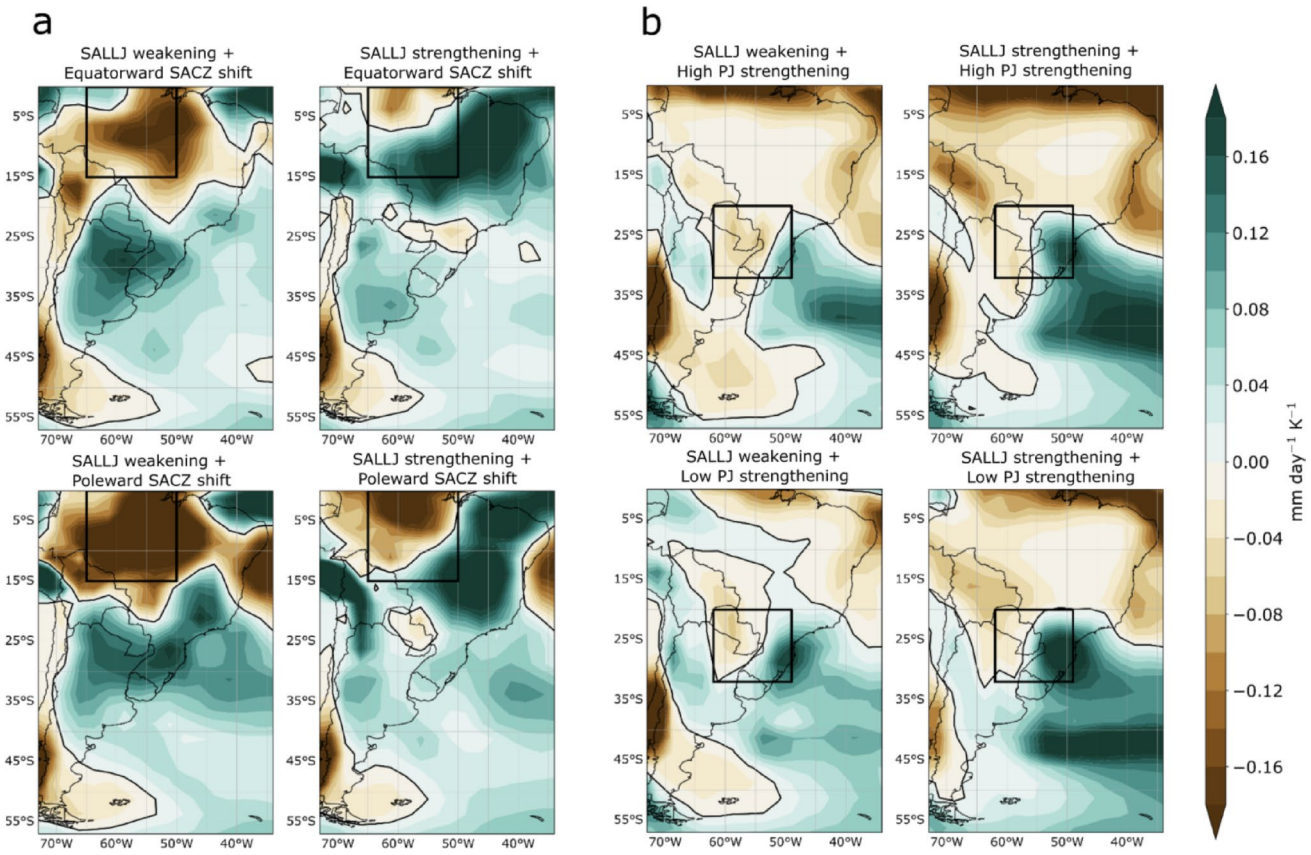

Fig. 7 Precipitation response per degree of warming (mm day^{-1} K^{-1}) associated with plausible storylines of climate change related to extreme values of South American Monsoon System changes in panel (**a**) and of extratropical cyclone changes in JJA in panel (**b**). The black rectangle in **a** is the Amazon basin (50°–65° W and 0°–15° S) and in b) La Plata basin (49°–62° W; 20°–32°S)

large SALLJ strengthening and equatorward SACZ shift, we see a cyclonic circulation over Argentina (Fig. S1a). This results in a more continental and closed circulation pattern, leading to southeasterly winds and a stronger SALLJ. This pattern can explain the enhanced moisture transport to the south/southeastern part of the Amazon basin, contributing to enhanced convection and precipitation associated with this extreme combination. On the other hand, southerly winds can be associated with dry conditions, since this pattern can contribute to trade winds weakening (Fig. S1a).

In summary, models project wet conditions in the Amazon basin during DJF only with SALLJ strengthening and an equatorward SACZ shift. This means that only one extreme combination indicates wet conditions for the Amazon basin across the models. The storyline phase space reveals many models aligned with the extreme storyline related to dry conditions over the Amazon basin. The SACZ poleward shift results in a dry response in the Amazon basin, a pattern associated with a wetter response in SESA.

Figure 7b shows the precipitation response to extreme combinations of SALLJ and polar jet changes for SL3, while Fig. S1b presents the circulation response at lower levels. The extreme combination of SALLJ weakening and high polar jet strengthening leads to a dry response, different from the others. The circulation response for these combinations illustrates an anticyclonic circulation between 35° and 45° S. The northeasterly wind from the western part of the anticyclonic circulation brings moisture and warm air from low latitudes and the ocean, resulting in wet conditions over the ocean. Meanwhile, the continent (a large part of the La Plata basin) experiences dry conditions due to the weak northwesterly wind associated with SALLJ (Fig. S1b, left/upper panel). The strengthening of the SALLJ in winter can lead to an increase in extratropical cyclones and in frontal systems' frequency and intensity, since this system needs moisture transport for maintenance (Reboita et al. 2012; Mendes et al. 2009; Gramcianinov et al. 2019). Because there is more coastal/oceanic precipitation, the wet response pattern appears to be related to the frontal system and extratropical pattern. Polar jets have a wet response over the adjacent ocean and the western part of the La Plata basin (Fig. 7b, right panel).

In summary, for SL3, the extreme combinations of the remote drivers for a SALLJ strengthening show a continental wet response over the La Plata basin. On the other hand, weaker SALLJ combinations show a slightly weaker wet response over the ocean and a dry response over the continent. This pattern shows that SALLJ plays a big role in the precipitation regime in future projections, as observed in the historical period.

3.3 Model selection

The criterion for selecting the models is defined by their spread in relation to the precipitation response in future climate through the circulation uncertainty, which is considered through three storyline sets (Fig. 8) and the validation of the models in the historical period through indices that summarise the main climatological patterns in SA (Fig. 6). Figure 8 presents the precipitation response for each combination of the storyline set (SL1, SL2 and SL3). The calculations are based on the linear regression for the storylines set and for each region. The final result of the precipitation response heatmap selects a subset of models that capture a range of future outcomes under both wet and dry conditions.

In this work, we combine the future outcomes information with the best representation of the climatological patterns in the historical period (final score in the last row, Fig. 6) and propose a methodology for the final best-fit model selection. In summary, we selected a range of models with different future possibilities, taking into account the three storyline sets together. For a conceptual example, if a range of models has wet conditions in SL1 and SL3 but dry in SL2, we refer to this as a future possibility named A. On the other hand, if a second range of models indicates dry conditions in SL1 and SL2, but wet conditions in SL3, we label this as a future possibility B. In principle, if we consider a wet and a dry change for each storyline set we could have eight combinations. We did not considered the same sign of change (wet or dry) is simultaneously projected for the three regions. Additionally, SL1 (LPB) never dries at the same time as SL2

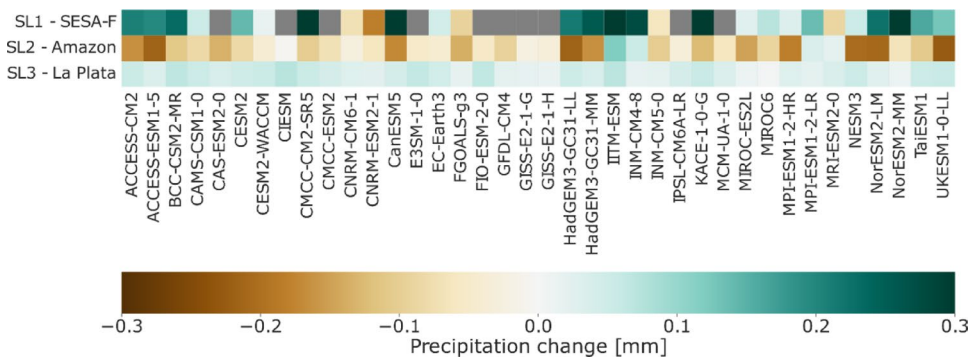

Fig. 8 Heatmap for the precipitation response estimated from the combination of the multimodel ensemble mean and the contributions associated with the remote driver responses using the multiple linear regression model of SL1, SL2 and SL3. The grey blocks represent models for which there are no values for SL1

Table 4 Best minimum model ensemble according to the model validation and storyline approach

Storylines	Wet	Dry
SL1 (SESA-F-DJF)	NorESM2-MM MIROC6 CMCC-CM2-SR5	MRI-ESM2-0
SL2 (AMZ-DJF)	MRI-ESM2-0	NorESM2-MM, CMCC-CM2-SR5 MIROC6
SL3 (LPB-JJA)	NorESM2-MM CMCC-CM2-SR5 MRI-ESM2-0	MIROC6

(AMZ) dries and vice versa. Hence, we only need to cover four possible and relevant combinations, which are represented by four models that have a good representation of the climatological patterns in the historical period.

Following this approach, the minimum ensemble of models that could represent wet and dry scenarios for all the regions is reported in Table 4 and Fig. 9. Two models (NorESM2-MM, CMCC-CM2-SR5) capture SL1 (wet), SL2 (dry) and SL3 (wet) changes; one (MIROC6) captures SL1 (wet), SL2 (dry) and SL3 (dry); and one (MRI-ESM2-0) SL1 (dry), SL2 (wet) and SL3 (wet). Figure 9 illustrates the chosen model's range across various parts of the phase space diagram, corresponding to the different plausible futures for the drivers that impact the SA domain. It is notable that the precipitation response for two extreme conditions (SALLJ weakening+equatorward SACZ shift and SALLJ weakening+poleward SACZ shift) is a dry response in AMZ in SL2, resulting in a plausible future model in just one quadrant in Fig. 9.

4 Final remarks

Regional Climate Models (RCMs) require Global Climate Models for the dynamical downscaling approach. Due to the misrepresentation of climatological features in some GCMs, it is crucial to select the best models for a specific region among the available GCMs. In this work we have presented a possible method based on model validation in the historical period and precipitation projections to account for uncertainty in precipitation responses in different regions and to be able to include a wide range of possible future outcomes.

Three storylines have been proposed for South America (SA) (SL1, SL2 and SL3), and a set of validation indices focused on the main large-scale circulation patterns over the region. The first circulation system is the South American Monsoon System (SAMS) in the Austral summer, and the second one involves extratropical cyclones in both the summer and winter seasons. In addition to that the South Atlantic Convergence Zone (SACZ), the South America Low-level Jet (SALLJ), trade winds, Bolivian High, northeast trough, upper-level jets and South Atlantic and Pacific subtropical high were analysed and indices have been proposed to

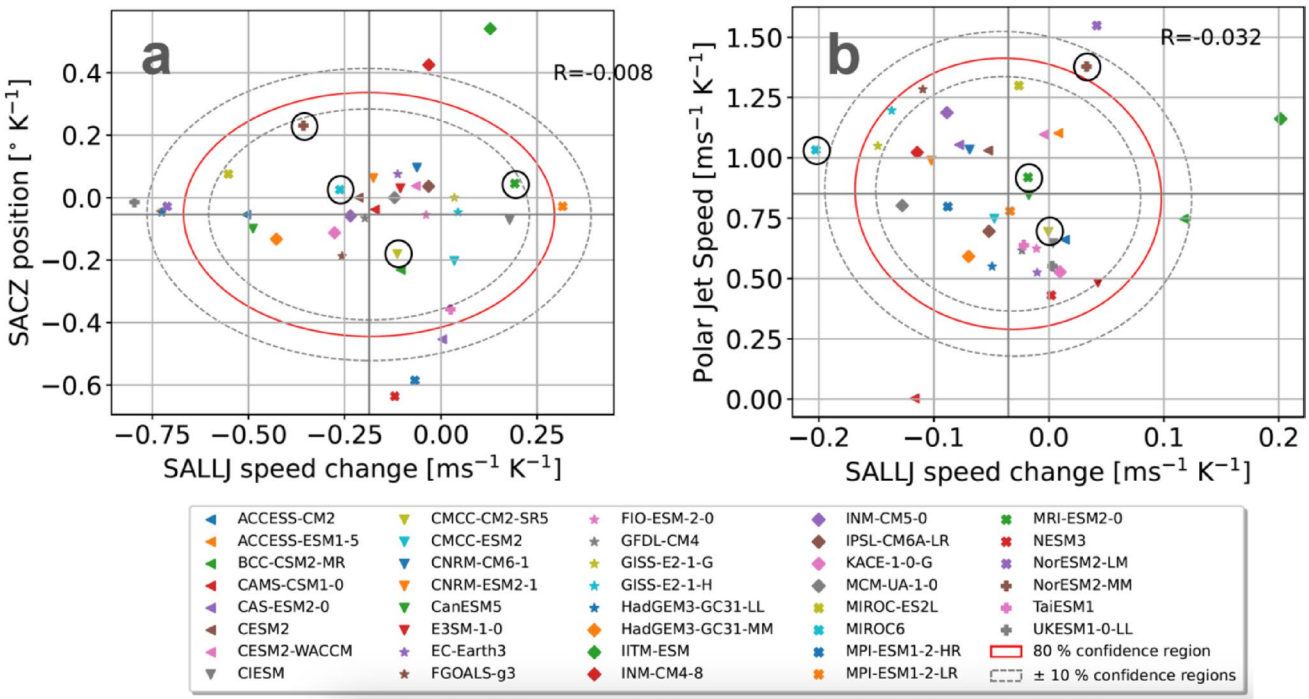

Fig. 9 Same as Fig. 5, but highlighting the selected models with a black circle

validate these dynamical drivers of the precipitation circulation regimes over SA.

Almost all CMIP6 GCMs have a good performance in representing the South Atlantic (Pacific) Subtropical high in both seasons. However, some models have difficulties in representing the SALLJ pattern in both seasons due to the Andes interaction with this system and the models' misrepresentation of topography. Upper-level regional circulation in summer is better represented than in winter. Additionally, CMIP6 GCMs show difficulties in representing the precipitation variability in austral summer, while almost all models perform well in representing the annual cycle of precipitation in all the regions used in the analysis.

In the first storyline set, the dry signal in SESA-F is connected with high upper-tropospheric tropical warming, an early stratospheric polar vortex breakdown and low tropical Pacific SSTs with respect to the ensemble mean (Mindlin et al. 2023). A high upper-tropospheric tropical warming drives an expansion of the Hadley cell, while an early stratospheric polar vortex breakdown represents a small shift of the westerly jet. The tropical SSTs influence this region via tropical-extratropical teleconnections. This configuration of large-scale responses leads to drier changes than those projected by the ensemble mean (Mindlin et al. 2023). In the second storyline set (SL2), a significant equatorward shift of the SACZ results in a wet or dry precipitation response depending on the SALLJ's strength over the Amazon basin. A SALLJ weakening with a small poleward shift of the SACZ position leads to a strong dry response over the Amazon basin. In the third storyline set (SL3), a wet precipitation response is observed over the La Plata Basin across all extreme combinations of regional drivers. The wet response is most intense when driven by SALLJ strengthening, consistent with the direct relationship between SALLJ intensity and precipitation over the La Plata basin (Berbery and Barros 2002; Nascimento et al. 2016). The stronger wet response is independent of the polar jet's position and strength, as it has less impact on the La Plata basin when the polar jet is stronger.

By using both the model selection criteria and the three storyline sets to define possible futures in the three specific regions (SESA-F, Amazon basin and La Plata basin), we propose a selection of models. We used the criteria to choose the best model for the historical validation for each of the two most extreme future storylines. The final minimal ensemble of models to guarantee the broader coverage of all the possible climate projections and best scoring for the representation of the large-scale circulation in South America is formed by four CMIP6 GCMs, namely NorESM2-MM, MIROC6, CMCC-CM2-SR5 and MRI-ESM2-0. This methodology is a proof of concept and can be used to either expand the minimal ensemble or can be applied to other regions making sure that fit for purpose storylines are used.

APPENDIX A

Assuming pattern scaling (Tebaldi and Arblaster 2014), the change in the target variable at each grid point x and for each model m, (ΔC_{xm}) is decomposed as $\Delta C_{xm} = P_{xm}\Delta T_m$. Where P_{xm} is the pattern change per degree of warming ΔT_m. Then, P_{xm} is modeled as a linear combination of remote driver responses.

$$P_{xm} = a_x + \sum_i^N b_{ix} \left(\Delta RD_i/\Delta T\right)'_m + e_{xm} \quad \text{(A1)}$$

where the intercept a_x results in the multimodel ensemble mean (MEM) and b_{ix} are the sensitivities of the pattern to one positive standard deviation in the driver responses $(\Delta RD_i/\Delta T)'_m$, N is the number of drivers considered, ' means that the index is standardized. e_{xm} are the errors, which quantify the remaining uncertainty not explained by the chosen drivers.

(b_{ix} coefficients in Eq. (1)).

$$\begin{aligned} &P_{x\,exSL} = a_x \pm b_{1x}t_s \pm b_{2x}t_s \\ &\text{and} \\ &P_{x\,interSL} = a_x \pm b_{1x}t_s \mp b_{2x}t_s \end{aligned} \quad \text{(A2)}$$

where the *exSL* are the extreme storylines with the drivers in the extremes of the distribution and *interSL* are the intermediate storylines where the indices contribute with opposite signs.

Supplementary Information The online version contains supplementary material available at https://doi.org/10.1007/s00382-025-08017-8.

Acknowledgements The authors would like to thank the Copernicus Climate Change Service, ECMWF. We acknowledge the World Climate Research Programme Working Group on Coupled Modelling and the modelling groups responsible for producing the simulations. A.A Cardoso thanks the STEP programme for supporting the sandwich fellowship and Coordenação de Aperfeiçoamento de Nível Superior (CAPES) for the fellowship in Brazil. JM funded by CONICET PhD grant, Microsoft Research PhD fellowship and the Saxon State Ministry for Science, Culture and Tourism (SMWK) – [3-7304/44/4-2023/8846].

Funding The Article Processing Charge (APC) for the publication of this research was funded by the Coordenação de Aperfeiçoamento de Pessoal de Nível Superior - Brasil (CAPES) (ROR identifier: 00x0ma614). This work was partially supported by FAPESP (2022/05476-2), Coordenação de Aperfeiçoamento de Pessoal de Nível Superior (CAPES), and Conselho Nacional de Desenvolvimento Científico e Tecnológico (CNPq Grants 430314/2018-3; 304949/2018-3), as well as the UNESO fellowship program in Italy.

Data availability Data from ERA5 (https://cds.climate.copernicus.eu/cdsapp#!/dataset/reanalysis-era5-single-levels?tab=form; Hersbach et al. 2020), were used in the creation of this manuscript. CMIP6 output available at https://esgf-node.llnl.gov/search/cmip6/. Figures were made with R (ggplot2, https://ggplot2.tidyverse.org; Wickham 2016) and Python (Matplotlib, https://matplotlib.org/; Caswell et al. 2021; Hunter 2007). CMIP analysis is done with ESMValTool (https://tutorial.esmvaltool.org/).

Declarations

Conflict of interest The authors do not have conflict of interest.

References

Arias PA, Correa IC, Fita L et al (2025) How well CMIP6 models simulate key boundary conditions affecting South American climate? Insights for regional modeling efforts. Clim Dyn 63:231. https://doi.org/10.1007/s00382-025-07704-w

Berbery EH, Barros VR (2002) The Hydrologic Cycle of the La Plata Basin in South America. J. Hydrometeor. 3:630–645.

Bombardi RJ, Carvalho LMV (2009) IPCC global coupled model simulations of the South America monsoon system. Clim Dyn 33(7–8):893–916

Butler AH, Thompson DWJ, Heikes R (2010) The steady-state atmospheric circulation response to climate change–like thermal forcings in a simple general circulation model. J Clim 23(13):3474–3496. https://doi.org/10.1175/2010jcli3228.1

Cardoso AA, da Rocha RP, Crespo NM (2022) Synoptic climatology of subtropical cyclone impacts on near-surface winds over the South Atlantic Basin. Earth Space Sci. https://doi.org/10.1029/2022ea002482

Carvalho LMV, Jones C, Liebmann B (2004) The South Atlantic Convergence Zone: intensity, form, persistence, and relationships with intraseasonal to interannual activity and extreme rainfall. J Clim 17(1):88–108. https://doi.org/10.1175/1520-0442(2004)017%3c0088:tsaczi%3e2.0.co;2

Caswell TA, Droettboom M, Lee A, De Andrade ES, Hoffmann T, Hunter J, Ivanov P(2021) matplotlib/matplotlib: REL: v3. 5.0. Zenodo.

Coelho CAS, de Souza DC, Kubota PY, Cavalcanti IFA, Baker JCA, Figueroa SN, Firpo MAF, Guimarães BS, Costa SMS, Gonçalves LJM, Bonatti JP, Sampaio G, Klingaman NP, Chevuturi A, Andrews MB (2021) Assessing the representation of South American monsoon features in Brazil and U.K. climate model simulations. Clim Resil Sustain. https://doi.org/10.1002/cli2.27

Crespo NM, da Rocha RP, Sprenger M, Wernli H (2020) A potential vorticity perspective on cyclogenesis over centre-eastern South America. Int J Climatol 41(1):663–678. https://doi.org/10.1002/joc.6644

Dai A (2006) Precipitation Characteristics in Eighteen Coupled Climate Models. J. Climate. 19:4605–4630. https://doi.org/10.1175/JCLI3884.1

da Rocha RP, Sugahara S, da Silveira RB (2004) Sea waves generated by extratropical cyclones in the South Atlantic Ocean: hindcast and validation against altimeter data. Weather Forecast 19(2):398–410. https://doi.org/10.1175/1520-0434(2004)019%3c0398:SWGBEC%3e2.0.CO;2

da Silva AE, de Carvalho LMV (2007) Large-scale index for South America Monsoon (LISAM). Atmos Sci Lett 8(2):51–57. https://doi.org/10.1002/asl.150

da Silva ML, de Oliveira CP, de Araújo JM, Silva CMSe (2022) Performance assessment of Coupled Model Intercomparison Project Phase 5 models in tropical South America using TOPSIS-based method. Int J Climatol 42(16):8290–8312. https://doi.org/10.1002/joc.7708

de Jesus EM, da Rocha RP, Crespo NM, Reboita MS, Gozzo LF (2020) Multi-model climate projections of the main cyclogenesis hot-spots and associated winds over the eastern coast of South America. Clim Dyn 56(1–2):537–557. https://doi.org/10.1007/s00382-020-05490-1

Di Virgilio G, Ji F, Tam E, Nishant N, Evans JP, Thomas C, Riley ML, Beyer K, Grose MR, Narsey S, Delage F (2022) Selecting CMIP6 GCMs for CORDEX dynamical downscaling: model performance, independence, and climate change signals. Earths Future. https://doi.org/10.1029/2021ef002625

Eyring V, Bony S, Meehl GA, Senior C, Stevens B, Stouffer RJ, Taylor KE (2016) Overview of the Coupled Model Intercomparison Project Phase 6 (CMIP6) experimental design and organisation. Copernic GmbH. https://doi.org/10.5194/gmd-9-1937-2016

Ferreira GWS, Reboita MS (2022) A new look into the South America precipitation regimes: observation and forecast. Atmosphere 13(6):873. https://doi.org/10.3390/atmos13060873

Giorgi F (2019) Thirty years of regional climate modeling: where are we and where are we going next? J Geophys Res Atmos 124(11):5696–5723. https://doi.org/10.1029/2018jd030094

Gramcianinov CB, Hodges KI, Camargo R (2019) The properties and genesis environments of South Atlantic cyclones. Clim Dyn 53(7–8):4115–4140. https://doi.org/10.1007/s00382-019-04778-1

Gulev S, Thorne P, Ahn J, Dentener F, Domingues C, Gerland S, Gong D, Kaufman D, Nnamchi H, Quaas J, Rivera J, Sathyendranath S, Smith S, Trewin B, von Schuckmann K, Vose R (2021) Changing state of the climate system, page 287–422. Cambridge University Press, Cambridge, New York

Harris I, Osborn TJ, Jones P, Lister D (2020) Version 4 of the CRU TS monthly high-resolution gridded multivariate climate dataset. Sci Data. https://doi.org/10.1038/s41597-020-0453-3

Hersbach H, Bell B, Berrisford P, Hirahara S, Horányi A, Muñoz-Sabater J, Nicolas J, Peubey C, Radu R, Schepers D, Simmons A, Soci C, Abdalla S, Abellan X, Balsamo G, Bechtold P, Biavati G, Bidlot J, Bonavita M, Thépaut J (2020) The ERA5 global reanalysis. Q J R Meteorol Soc 146(730):1999–2049. https://doi.org/10.1002/qj.3803

Hoskins BJ, Hodges KI (2005) A new perspective on Southern Hemisphere storm tracks. J Climate 18(20):4108–4129. https://doi.org/10.1175/jcli3570.1

Hunter JD (2007) Matplotlib: A 2D graphics environment. Computing in Science & Engineering. 9(3):90-95. https://doi.org/10.5281/zenodo.592536

Intergovernmental Panel on Climate Change (IPCC) (2023) Climate change 2021 – the physical science basis. Cambridge University Press, Cambridge. https://doi.org/10.1017/9781009157896

Jones C (2019) Recent changes in the South America low-level jet. Npj Clim Atmos Sci. https://doi.org/10.1038/s41612-019-0077-5

Jones C, Carvalho LMV (2002) Active and break phases in the South American monsoon system. J Clim 15(8):905–914. https://doi.org/10.1175/1520-0442(2002)015%3c0905:aabpit%3e2.0.co;2

Kodama Y (1992) Large-scale common features of subtropical precipitation zones (the Baiu Frontal Zone, the SPCZ, and the SACZ) part I: characteristics of subtropical frontal zones. J Meteorol Soc Jpn Ser II 70(4):813–836. https://doi.org/10.2151/jmsj1965.70.4_813

Kodama Y-M (1993) Large-scale common features of sub-tropical convergence zones (the baiu frontal zone, the SPCZ, and the SACZ) part II: conditions of the circulations for generating the stczs. J Meteorol Soc Jpn Ser II 71(5):581–610. https://doi.org/10.2151/jmsj1965.71.5_581

Liebmann B, Vera CS, Carvalho LMV, Camilloni IA, Hoerling MP, Allured D, Barros VR, Báez J, Bidegain M (2004) An observed trend in Central South American precipitation. J Clim 17(22):4357–4367. https://doi.org/10.1175/3205.1

Llopart M, Coppola E, Giorgi F, da Rocha RP, Cuadra SV (2014) Climate change impact on precipitation for the Amazon and La Plata basins. Clim Change 125(1):111–125. https://doi.org/10.1007/s10584-014-1140-1

Lu J, Vecchi GA, Reichler T (2007) Expansion of the Hadley cell under global warming. Geophys Res Lett. https://doi.org/10.1029/2006gl028443

Manzini E, Karpechko AY, Anstey J, Baldwin MP, Black RX, Cagnazzo C, Calvo N, Charlton-Perez A, Christiansen B, Davini P, Gerber E, Giorgetta M, Gray L, Hardiman SC, Lee Y-Y, Marsh DR, McDaniel BA, Purich A, Scaife AA, Shindell D, Son S-W, Watanabe S, Zappa G (2014) Northern winter climate change: assessment of uncertainty in CMIP5 projections related to stratosphere-troposphere coupling. J Geophys Res Atmos 119(13):7979–7998. https://doi.org/10.1002/2013jd021403

Marengo JA, Liebmann B, Grimm AM, Misra V, Silva Dias PL, Cavalcanti IFA, Carvalho LMV, Berbery EH, Ambrizzi T, Vera CS, Saulo AC, Nogues-Paegle J, Zipser E, Seth A, Alves LM (2010) Recent developments on the South American monsoon system. Int J Climatol 32(1):1–21. https://doi.org/10.1002/joc.2254

Marengo JA, Soares WR, Saulo C, Nicolini M (2004) Climatology of the low-level jet east of the Andes as derived from the NCEP–NCAR reanalyses: characteristics and temporal variability. J Clim 17(12):2261–2280. https://doi.org/10.1175/1520-0442(2004)017%3c2261:COTLJE%3e2.0.CO;2

McSweeney CF, Jones RG, Lee RW, Rowell DP (2015) Selecting CMIP5 GCMs for downscaling over multiple regions. Clim Dyn 44(11–12):3237–3260. https://doi.org/10.1007/s00382-014-2418-8

Mendes D, Souza EP, Marengo JA, Mendes MCD (2009) Climatology of extratropical cyclones over the South American–southern oceans sector. Theor Appl Climatol 100(3–4):239–250. https://doi.org/10.1007/s00704-009-0161-6

Mindlin J, Shepherd TG, Vera CS, Osman M, Zappa G, Lee RW, Hodges KI (2020) Storyline description of Southern Hemisphere midlatitude circulation and precipitation response to greenhouse gas forcing. Clim Dyn 54(9–10):4399–4421. https://doi.org/10.1007/s00382-020-05234-1

Mindlin J, Vera CS, Shepherd TG, Osman M (2023) Plausible Drying and Wetting Scenarios for Summer in Southeastern South America. J. Climate. 36:7973–7991. https://doi.org/10.1175/JCLI-D-23-0134.1

Montini TL, Jones C, Carvalho LMV (2019) The South American low-level jet: a new climatology, variability, and changes. J Geophys Res Atmos 124(3):1200–1218. https://doi.org/10.1029/2018jd029634

Narsey S, Brown JR, Delage F, Boschat G, Grose M, Colman R, Power S (2022) Storylines of South Pacific convergence zone changes in a warmer world. J Clim 35(20):2949–2967. https://doi.org/10.1175/jcli-d-21-0433.1

Nascimento MG, Herdies DL, de Souza DO (2016) The South American Water Balance: The Influence of Low-Level Jets. Journal of Climate, 29(4):1429-1449. https://doi.org/10.1175/JCLI-D-15-0065.1

Olmo ME, Espinoza J-C, Bettolli ML, Sierra JP, Junquas C, Arias PA et al (2022) Circulation patterns and associated rainfall over south tropical South America: GCMs evaluation during the dry-to-wet transition season. J Geophys Res: Atmos 127:e2022JD036468. https://doi.org/10.1029/2022JD036468

Palmer TE, McSweeney CF, Booth BBB, Priestley MDK, Davini P, Brunner L, Borchert L, Menary MB (2023) Performance-based sub-selection of CMIP6 models for impact assessments in Europe. Earth Syst Dyn 14(2):457–483. https://doi.org/10.5194/esd-14-457-2023

Reboita MS, Ambrizzi T, Silva BA, Pinheiro RF, da Rocha RP (2019) The south atlantic subtropical anticyclone: present and future climate. Front Earth Sci. https://doi.org/10.3389/feart.2019.00008

Reboita MS, da Rocha RP, Ambrizzi T (2012) Dynamic and climatological features of cyclonic developments over southwestern South Atlantic Ocean. In: Veress B, Szigethy J (eds) Horizons in earth science research. Nova Science Publishers Inc, New York, pp 135–160

Reboita MS, da Rocha RP, Ambrizzi T, Sugahara S (2010a) South Atlantic Ocean cyclogenesis climatology simulated by regional climate model (RegCM3). Clim Dyn 35(7–8):1331–1347. https://doi.org/10.1007/s00382-009-0668-7

Reboita MS, Gan MA, da Rocha RP, Ambrizzi T (2010b) Precipitation regimes in south america: a bibliography review. Rev Bras Meteor 25:185–204

Rivière G (2011) A dynamical interpretation of the poleward shift of the jet streams in global warming scenarios. J Atmos Sci 68(6):1253–1272. https://doi.org/10.1175/2011jas3641.1

Schmidt DF, Grise KM (2017) The response of local precipitation and sea level pressure to Hadley Cell expansion. Geophys Res Lett. https://doi.org/10.1002/2017gl075380

Shepherd TG (2014) Atmospheric circulation as a source of uncertainty in climate change projections. Nat Geosci 7(10):703–708. https://doi.org/10.1038/ngeo2253

Shepherd TG, Boyd E, Calel RA, Chapman SC, Dessai S, Dima-West IM, Fowler HJ, James R, Maraun D, Martius O, Senior CA, Sobel AH, Stainforth DA, Tett SFB, Trenberth KE, van den Hurk BJJM, Watkins NW, Wilby RL, Zenghelis DA (2018) Storylines: an alternative approach to representing uncertainty in physical aspects of climate change. Clim Change 151(3–4):555–571. https://doi.org/10.1007/s10584-018-2317-9

Silva VBS, Kousky VE (2012) The South American monsoon system: climatology and variability. Mod Climatol 123:152. https://doi.org/10.5772/38565

Soares WR, Marengo JA (2008) Assessments of moisture fluxes east of the Andes in South America in a global warming scenario. Int J Climatol 29(10):1395–1414. https://doi.org/10.1002/joc.1800

Sun Y, Solomon S, Dai A, Portmann RW (2006) How Often Does It Rain?. J. Climate. 19:916–934. https://doi.org/10.1175/JCLI3672.1

Tebaldi C, Arblaster JM (2014) Pattern scaling: Its strengths and limitations, and an update on the latest model simulations. Climatic Change. 122:459–471. https://doi.org/10.1007/s10584-013-1032-9

Torres-Alavez JA, Das S, Corrales-Suastegui A, Coppola E, Giorgi F, Raffaele F, Bukovsky MS, Ashfaq M, Salinas JA, Sines T (2021) Future projections in the climatology of global low-level jets from

CORDEX-CORE simulations. Clim Dyn 57(5–6):1551–1569. https://doi.org/10.1007/s00382-021-05671-6

Vera C, Baez J, Douglas M, Emmanuel CB, Marengo J, Meitin J, Nicolini M, Nogues-Paegle J, Paegle J, Penalba O, Salio P, Saulo C, Silva Dias MA, Dias PS, Zipser E (2006a) The South American low-level jet experiment. Bull Am Meteorol Soc 87(1):63–78. https://doi.org/10.1175/bams-87-1-63

Vera C, Higgins W, Amador J, Ambrizzi T, Garreaud R, Gochis D, Gutzler D, Lettenmaier D, Marengo J, Mechoso CR, Nogues-Paegle J, Silva Dias PL, Zhang C (2006b) Toward a unified view of the American monsoon systems. J Clim 19(20):4977–5000

Wickham H (2016) Ggplot2: Elegant graphics for data analysis (2nd ed.). Springer International Publishing.

Zappa G, Shepherd TG (2017) Storylines of atmospheric circulation change for European regional climate impact assessment. J Clim 30(16):6561–6577. https://doi.org/10.1175/jcli-d-16-0807.1

Zhang MZ, Xu Z, Han Y et al (2024) Evaluation of CMIP6 models toward dynamical downscaling over 14 CORDEX domains. Clim Dyn 62:4475–4489. https://doi.org/10.1007/s00382-022-06355-5

Zilli MT, Carvalho LMV (2021) Detection and attribution of precipitation trends associated with the poleward shift of the South Atlantic Convergence Zone using CMIP5 simulations. Int J Climatol 41(5):3085–3106. https://doi.org/10.1002/joc.7007

Zilli MT, Carvalho LMV, Liebmann B, Silva Dias MA (2017) A comprehensive analysis of trends in extreme precipitation over southeastern coast of Brazil. Int J Climatol 37(5):2269–2279. https://doi.org/10.1002/joc.4840

Zilli MT, Carvalho LMV, Lintner BR (2018) The poleward shift of South Atlantic Convergence Zone in recent decades. Clim Dyn 52(5–6):2545–2563. https://doi.org/10.1007/s00382-018-4277-1